

Article

Application of Fractional Derivative Without Singular and Local Kernel to Enhanced Heat Transfer in CNTs Nanofluid Over an Inclined Plate

Muhammad Saqib ¹, Abdul Rahman Mohd Kasim ², Nurul Farahain Mohammad ³,
Dennis Ling Chuan Ching ⁴ and Sharidan Shafie ^{1,*}

¹ Department of Mathematical Sciences, Faculty of Science, Universiti Teknologi Malaysia JB, Johor Bahru 81310, Malaysia; muhammadsaqib621@gmail.com

² Centre of Mathematical Sciences, Universiti Malaysia Pahang, 26300, Lebuhraya Tun Razak' Gambang, Kuantan Pahang 25200, Malaysia; rahmanmohd@ump.edu.my

³ Department of Computational and Theoretical Sciences' International Islamic Universiti Malaysia, Kuantan Pahang 25200, Malaysia; farahain@iium.edu.my

⁴ Fundamental and Applied Sciences Department, Universti Teknologi PETRONAS, Perak 32610, Malaysia; dennis.ling@utp.edu.my

* Correspondence: sharidan@utm.my

Received: 19 March 2020; Accepted: 10 April 2020; Published: 6 May 2020



Abstract: Nanofluids are a novel class of heat transfer fluid that plays a vital role in industries. In mathematical investigations, these fluids are modeled in terms of traditional integer-order partial differential equations (PDEs). It is recognized that traditional PDEs cannot decode the complex behavior of physical flow parameters and memory effects. Therefore, this article intends to study the mixed convection heat transfer in nanofluid over an inclined vertical plate via fractional derivatives approach. The problem in hand is modeled in connection with Atangana–Baleanu fractional derivatives without singular and local kernel with a strong memory. Human blood is considered as base fluid and carbon nanotube (CNTs) (single-wall carbon nanotubes (SWCNTs) and multi-wall carbon nanotubes (MWCNTs)) are dispersed into it to form blood-CNTs nanofluid. The nanofluid is considered to flow in a saturated porous medium under the influence of an applied magnetic field. The exact analytical expressions for velocity and temperature profiles are acquired using the Laplace transform technique and plotted in various graphs. The empirical results indicate that the memory effect decreases with increasing fractional parameters in the case of both temperature and velocity profiles. Moreover, the temperature profile is higher for blood SWCNTs because of higher thermal conductivity whereas this trend is found opposite in the case of velocity profile due to densities difference.

Keywords: enhance heat transfer; nanofluids; CNTs; fractional derivatives; Laplace transform

1. Introduction

In mixed convection regimes, enhanced heat transfer is significant for energy-saving operations in industries. The primary constraint of traditional heat transfer fluid is poor thermal conductivity which influences the mixed convection process [1]. Overcoming the flaws of traditional heat transfer fluids, nanofluid is a novel category of fluids that play its role in altering thermal features of traditional fluids as illustration water, oils, alcohol, and ethylene glycol [2,3]. Surveys have indicated that the usage of nanofluids results in the progress of the execution of heat coolant of electronics and heat exchangers [4–6]. The procedure of heat transfer alteration can be taken into account by use of a porous medium, employment of magnetic field, and amending the thermophysical properties through

nanomaterials (for instance, oxide, silica, carbid, metals, non-metals, graphene, and carbon nano tubes (CNTs) nanometer-sized particles) [7]. The contemporary use of nanofluids and forces, for example, magnetic fields and porous media to strengthen the thermal properties of heat exchangers, have been debated in the literature.

Alzahrani et al. [8] studied single-wall carbon nanotubes (SWCNTs) and multi-wall carbon nanotubes (MWCNT) in water as a base fluid within parallel horizontal rotating plates. The inertia characteristics, microstructure, heat absorption/consumption, and thermal radiation are assumed. The problem is modeled in the form of partial differential equations (PDEs), then is transformed into ordinary differential equations (ODEs) and handled with the Homotopy Analysis Method (HAM). It was indicated that the velocity profile decreases with increasing volume concentration whereas the temperature profiles behave in a reverse way. Gul et al. [9] examined the flow of water-based SWCNT and MWCNT nanofluids with variable temperature over a needle. The principal equations of the problem were modeled in the form of Caputo fractional derivatives and solved for numerical solutions. They pointed out that the impact of numerous physical flow parameters is restricted in the case of traditional derivatives. However, in the case of Caputo fractional derivatives, the influence of these parameters is diverse at contrary intervals. Hassanian et al. [10] investigated the flow of oil-CNT (SWCNT and MWCNT) nanofluid over a stretching sheeting along with magnetohydrodynamic (MHD) and radiations effects. It was noticed that energy enhancement in oil-SWCNTs was higher than oil-MWCNTs due to high thermal conductivity, but the trend was opposite for velocity profiles due to the differences in densities. Jabbari et al. [11] analyzed the viscosity of water-based SWCNTs by means of equilibrium molecular dynamics simulation. The viscosity variation was made for 0.125%–0.734% SWCNTs nanofluids at temperature 25–65 °C. They reported that the viscosity of nanofluid increases with a high-volume fraction of SWCNTs at low temperatures. Kumam et al. [12] carried out entropy generation and the second law of thermodynamics application for kerosene oil-SWCNTs and kerosene oil-MWCNTs flow in a rotating microchannel. They considered source/sink, radiation, and magnetic field effect. Their results shown that the velocity function reduced with Reynolds number and entropy generation increases with Reynolds and Brinkman numbers. The interesting applications of CNTs nanofluid can be found in review papers [13–15] and the reference therein.

CNTs feature considerable mechanical and electrical thermal conduction forming a hexagonal cylinder network of carbon atoms 100 nm in length and 1 nm in the bore. The major application of CNTs is listed as additives in polymers, nanolithography, hydrogen storage, supercapacitors, lithium battery anodes, and drug delivery [16]. Murshed [17] mentioned in the review paper that CNT nanofluids have six times higher thermal conductivity compared to other materials at ambient temperature. CNT nanofluids are sufficiently investigated in the literature (see, for example, Xie et al. [18], Sarafraz et al. [19], Selimefendigil, and Öztop [20], Ghazali et al. [21] and Abdeen et al. [22]) but without memory and heredity effects. This is since, in mathematical studies, the traditional models with integer-order PDEs are used. These models can be improved by using the applications of fractional derivatives. It is approved in the previous literature that fractional derivative models can explain efficiently the real-world problems comprising electrical networks, diffusive transport, probability, electromagnetic theory, rheology, viscoelastic materials, and fluid flow [23–29]. In the literature, several approaches for fractional derivatives are presented, but the most common are the Riemann–Liouville [30], the Caputo [31,32], the Caputo–Fabrizio [33] and Atangana–Baleanu [34] fractional derivatives approaches. Among them, the most recent is Atangana–Baleanu fractional derivative without local and singular kernel with strong heredity and memory effect.

For the problem in hand, the Atangana–Baleanu fractional derivative approach is chosen due to non-locality, non-singularity, and strong heredity and memory effect. A fractional Casson fluid model is developed for human blood CNT nanofluid associated with physical initial and boundary conditions. The model is solved for exact solutions via the Laplace transform technique. The analytical results are displayed in graphs with physical arguments.

2. Description of the Proposed Model

Consider the unsteady mixed convection flow of blood-based CNT nanofluid over an inclined vertical plate with isothermal temperature T_∞ (room temperature/ambient temperature). The half-space of the plate is packed with human blood with SWCNTs and MWCNTs nanofluids saturated in a porous medium. The nanofluid is assumed to be electrically conducting. Hence, a magnetic field $\sigma_{nf} B_0^2 \sin(\gamma)$ of strength B_0 and direction γ is applied to the flow direction. The induced magnetic field due to polarization is ignored because of a very small Reynolds number. At the beginning at $t \leq 0$, the system is in the rest position. However, after the short interval of time $t = 0^+$, the inclined plate oscillates with $U_0 H(t) \cos(\omega t)$ and the ambient temperature of the plate T_∞ rises to T_W . By virtue of a rise in temperature and oscillation of the plate, the mixed convection uncoils and the nanofluid starts motion in the upper direction, as exhibited in Figure 1.

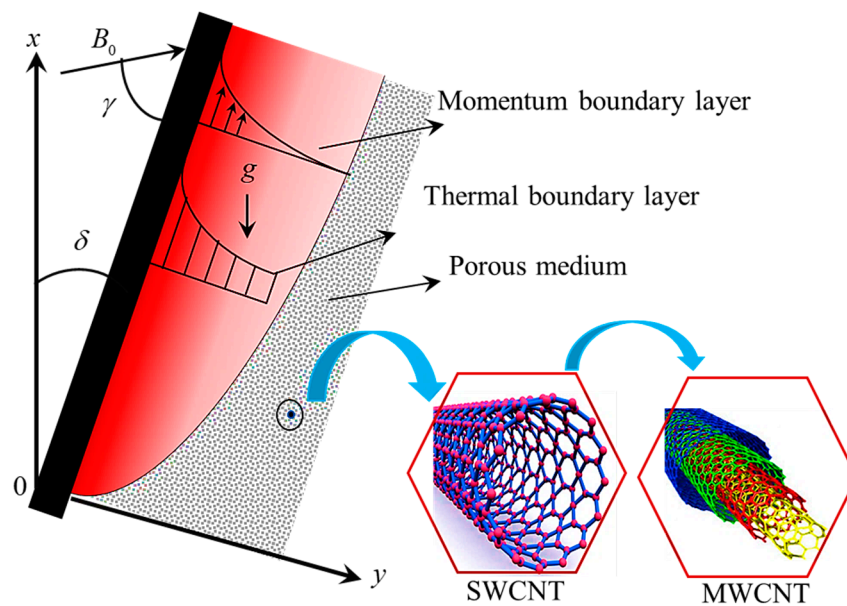


Figure 1. Configuration and coordinates system.

In the proposed problem, the Casson fluid model is subjected to blood and CNT nanoparticles are dispersed into it for enhanced heat transfer. The rheological relation and Cauchy stress tensor of Casson fluid is given as [35,36]

$$\mathbf{T} = \begin{cases} 2 \left(\mu_B + \frac{p_r}{\sqrt{2} \pi} \right) e_{ij}, & \pi > \pi_c \\ 2 \left(\mu_B + \frac{p_r}{\sqrt{2} \pi_c} \right) e_{ij}, & \pi < \pi_c \end{cases}, \quad (1)$$

where μ_B is the plastic dynamic viscosity, p_r is the yield stress and π_c is the critical values of the product of μ_b , and p_r . By virtue of Equation (1) along with the momentum equation, the Maxwell set of equations [37], Darcy’s law [38], Fourier law of heat conduction [39], and Boussinesq approximation [40] the governing equations of the proposed problem are given by [36]

$$\rho_{nf} \frac{\partial u(y,t)}{\partial t} = \mu_{nf} \left(1 + \frac{1}{\beta_0} \right) \frac{\partial^2 u(y,t)}{\partial y^2} - \left\{ \sigma_{nf} B_0^2 \sin \gamma + \left(1 + \frac{1}{\beta_0} \right) \frac{\mu_{nf} \varphi}{k} \right\} u(y,t) + g(\rho \beta_T)_{nf} (T(y,t) - T_\infty) \cos \delta, \quad (2)$$

$$(\rho C_p)_{nf} \frac{\partial T(y,t)}{\partial t} = k_{nf} \frac{\partial^2 T(y,t)}{\partial y^2}, \quad (3)$$

subject to the following initial and boundary conditions

$$u(y, 0) = 0, T(y, 0) = T_\infty, \forall y \geq 0, \tag{4}$$

$$\left. \begin{aligned} u(0, t) &= U_0 H(t) \cos \omega t, T(0, t) = T_W, \text{ for } t > 0 \\ u(y, t) &\rightarrow 0, T(y, t) \rightarrow T_\infty; y \rightarrow \infty, \text{ for } t > 0 \end{aligned} \right\} \tag{5}$$

where ρ_{nf} is the density, $u(y, t)$ is the velocity, μ_{nf} is the dynamic viscosity, β_0 is the Casson fluid parameter, σ_{nf} is the electrical conductivity, ϕ ($0 < \phi < 1$) is the porosity, k is the permeability, g is the gravitational acceleration, β_T is the thermal expansion, $T(y, t)$ is the temperature, $(C_p)_{nf}$ is the heat capacitance and k_{nf} is the thermal conductivity. The subscript nf is used for nanofluid where the subscripts f and s are used for base fluid and solid nanoparticles respectively. The mathematical models for the thermophysical properties of nanofluid are given in Table 1 whereas its numerical values are given in Table 2.

Table 1. Model for thermophysical properties of nanofluid [41].

Physical Quantity	Mathematical Model
Density	$\rho_{nf} = (1 - \phi)\rho_f + \phi\rho_s$
Dynamic viscosity	$\mu_{nf} = \frac{\mu_f}{(1-\phi)^{2.5}}$
Electrical conductivity	$\sigma_{nf} = \left\{ 1 + \frac{3\left(\frac{\sigma_s}{\sigma_f} - 1\right)\phi}{\left(\frac{\sigma_s}{\sigma_f} + 2\right) - \left(\frac{\sigma_s}{\sigma_f} - 1\right)\phi} \right\} \sigma_f$
Thermal expansion	$(\rho\beta_T)_{nf} = (1 - \phi)(\rho\beta_T)_f + \phi(\rho\beta_T)_s$
Heat capacitance	$(\rho C_p)_{nf} = (1 - \phi)(\rho C_p)_f + \phi(\rho C_p)_s$
Thermal conductivity	$k_{nf} = \left\{ \frac{(1-\phi) + 2\phi \frac{k_s}{k_s - k_f} \ln \frac{k_s - k_f}{2k_f}}{(1-\phi) + 2\phi \frac{k_s}{k_s - k_f} \ln \frac{k_s + k_f}{2k_f}} \right\} k_f$

Table 2. Values of thermophysical properties of base fluid and nanoparticles [36].

Material	Base Fluid	Nanoparticles	
	Human Blood	SWCNTs	MWCMTs
$\rho(\text{kg/m}^3)$	1053	2600	1600
$C_p(\text{J/kg K})$	3594	425	796
$k(\text{W/m K})$	0.492	6600	3000
$\beta_T \times 10^{-5}(\text{K}^{-1})$	0.8	$10^{-6} - 10^{-7}$	1.9×10^{-4}
σ	0.18	21	44

3. Methodology

In this study, the Laplace transform is used to acquire exact solutions of the considered problem. Primarily, the proposed model is transformed into a dimensionless form with an eye to reducing the number of variables and eradicating unity for clarity. Then, the dimensionless governing equations are artificially transformed into time-fractional Atangana–Baleanu fractional derivatives. The Atangana–Baleanu fractional Casson nanofluid model deals with the Laplace transform technique to generate exact solutions for velocity and temperature profiles. The obtained results are displayed in numerous graphs and discussed physically as presented in Figure 2.

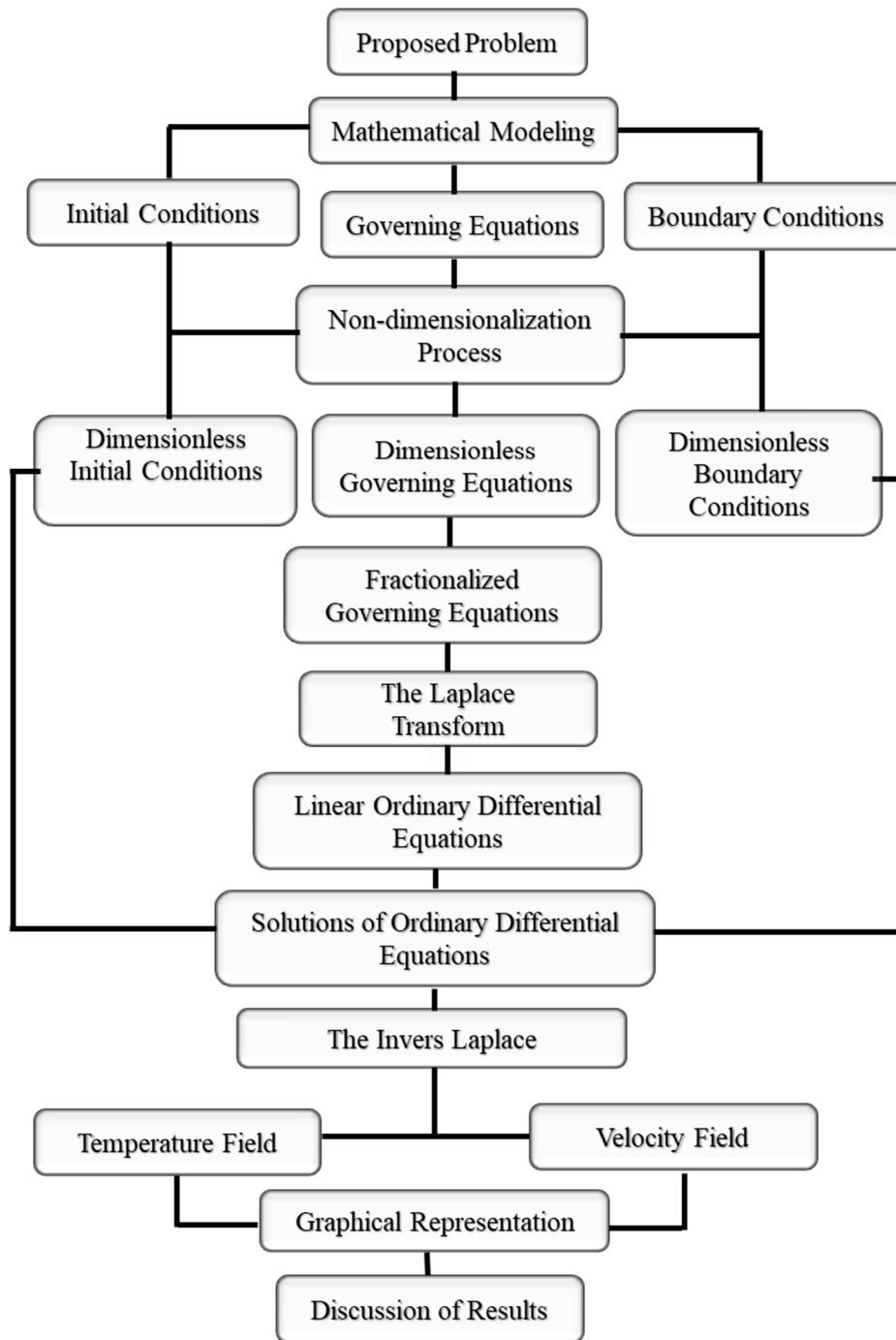


Figure 2. Operational framework.

Now, incorporate the following dimensionless variables

$$u^* = \frac{u}{u_0}, y^* = \frac{u_0}{v_f}, t^* = \frac{u_0^2}{v_f} t, \theta = \frac{T - T_\infty}{T_W - T_\infty}$$

into Equations (2)–(5), which yield to

$$\phi_0 \frac{\partial u(y, t)}{\partial t} = \frac{\phi_1}{\beta} \frac{\partial^2 u(y, t)}{\partial y^2} - \left(\phi_2 M \sin \gamma + \frac{\phi_3}{K} \right) u(y, t) + \phi_4 Gr \theta(y, t) \cos \delta, \tag{6}$$

$$\phi_5 \text{Pr} \frac{\partial \theta(y, t)}{\partial t} = \phi_6 \frac{\partial^2 \theta(y, t)}{\partial y^2}, \quad (7)$$

$$t \leq 0 : u(y, 0) = 0, \theta(y, 0) = 0, \forall y \geq 0, \quad (8)$$

$$\left. \begin{aligned} u(0, t) = H(t) \cos \omega t, \theta(0, t) = 1, \text{ for } t > 0 \\ u(y, t) \rightarrow 0, \theta(y, t) \rightarrow 0; t \rightarrow \infty, \text{ for } t > 0 \end{aligned} \right\} \quad (9)$$

where

$$\beta = \frac{\beta_0}{1 + \beta_0}, M = \frac{\nu_f \sigma_f B_0^2}{\rho_f U_0^2}, K = \frac{ku_0^2}{\nu_f \varphi}, Gr = \frac{g(\nu \beta_T)_f (T_W - T_\infty)}{u_0^3}, \text{Pr} = \left(\frac{\mu C_p}{k} \right)_f$$

$$\phi_0 = (1 - \phi_{nf}) + \frac{\phi \rho_s}{\rho_f}, \phi_1 = \frac{1}{1 - \phi}, \phi_2 = \frac{\sigma_{hnf}}{\sigma_f}, \phi_3 = (1 - \phi) + \frac{\phi(\rho \beta_T)_s}{(\rho \beta_T)_f},$$

$$\phi_4 = (1 - \phi) + \frac{\phi(\rho C_p)_s}{(\rho C_p)_f}, \phi_5 = \frac{k_{nf}}{k_f}$$

is the dimensionless Casson fluid parameter, magnetic number, permeability parameter, thermal Grashof number, and Prandtl number, respectively, and $\phi_0, \phi_1, \phi_2, \phi_3, \phi_4$, and ϕ_5 are constant terms produced during calculi. The time-fractional form of Equations (6) and (7) is given by [42,43]

$$\phi_0 {}^{AB} \mathcal{D}_t^\alpha u(y, t) = \frac{\phi_1}{\beta} \frac{\partial^2 u(y, t)}{\partial y^2} - \left(\phi_2 M \sin \gamma + \frac{\phi_1}{K} \right) u(y, t) + \phi_3 Gr \theta(y, t) \cos \delta; 0 < \alpha \leq 1, \quad (10)$$

$$\phi_4 \text{Pr} {}^{AB} \mathcal{D}_t^\alpha \theta(y, t) = \phi_5 \frac{\partial^2 \theta(y, t)}{\partial y^2}; 0 < \alpha \leq 1, \quad (11)$$

where ${}^{AB} \mathcal{D}_t^\alpha(\dots)$ is the Atangana–Baleanu time-fractional operator defined by [34]

$${}^{AB} \mathcal{D}_\tau^\alpha f(\eta, \tau) = \frac{N(\alpha)}{1 - \alpha} \int_0^\tau E_\alpha \left\{ \frac{-\alpha(\tau - t)^\alpha}{1 - \alpha} \right\} f'(\eta, \tau) dt; 0 < \alpha \leq 1, \quad (12)$$

where

$$E_\alpha(-t^\alpha) = \sum_{K=0}^{\infty} \frac{(-t)^{\alpha K}}{\Gamma(\alpha K + 1)} \quad (13)$$

is the non-local and non-singular Mittag–Leffler function used as the kernel in the construction of Equation (12). The Laplace transform of Equation (12) is given by [44]

$$\mathcal{L}\{f(\eta, \tau); q\} = \frac{q^\alpha \mathcal{L}\{f(\eta, \tau)\} - f(\eta, 0)}{(1 - \alpha)q^\alpha + \alpha}; 0 < \alpha \leq 1 \quad (14)$$

where $\mathcal{L}\{f(\eta, \tau)\} = \bar{f}(\eta, q)$ is the Laplace transform of $f(\eta, \tau)$ in the Laplace transform domain and $f(\eta, 0)$ is the initial values of $f(\eta, \tau)$. It worth mentioning here that for $\alpha = 1$, the model presented in Equations (10) and (11) can be reduced back to the classical form exhibited in Equations (2) and (3) which validated the time-fractional model proposed for CNT blood nanofluid.

4. Solutions of the Problem

The Laplace transform technique is adopted to find the exact solutions for the proposed problem.

4.1. Solution of Energy Equation

Applying the Laplace transform to Equation (11) in the light of Equations (12) and (14) and using the corresponding initial condition from Equations (8) yield to:

$$\frac{\partial^2 \bar{\theta}(y, q)}{\partial y^2} - \frac{\phi_4 \text{Pr}}{\phi_5} \frac{q^\alpha \bar{\theta}(y, q)}{(1 - \alpha)q^\alpha + \alpha} = 0; 0 < \alpha \leq 1. \tag{15}$$

The analytical solution of the homogeneous Equation (15) is given by:

$$\bar{\theta}(y, q) = \frac{1}{q} \exp\left(-y \sqrt{\frac{\phi_4 \text{Pr}}{\phi_5} \frac{q^\alpha}{(1 - \alpha)q^\alpha + \alpha}}\right); 0 < \alpha \leq 1. \tag{16}$$

Equations (16) is written in a more convenient form as:

$$\bar{\theta}(y, q) = \bar{\chi}(q) \bar{\psi}(\xi, q; a_2, a_3); 0 < \alpha \leq 1, \tag{17}$$

where

$$\bar{\psi}(y, q; a_2, a_3) = \frac{1}{q^\alpha} \exp\left(-y \sqrt{\frac{a_2 q^\alpha}{q^\alpha + a_3}}\right), \tag{18}$$

$$\bar{\chi}(q) = \frac{1}{q^{1-\alpha}}, \tag{19}$$

and

$$a_0 = \frac{\phi_4 \text{Pr}}{\phi_5}, a_1 = \frac{1}{1 - \alpha}, a_2 = a_0 a_1, a_3 = a_1 \alpha$$

The solution of the energy equation in the Laplace transform domain is given in Equation (17). Applying the inverse Laplace transform to Equation (17) yield to:

$$\theta(y, t) = \int_0^t \chi(t - \tau) \psi(y, \tau; a_2, a_3) d\tau; 0 < \alpha \leq 1, \tag{20}$$

Equation (20) represents the final solutions of the energy equation in terms of convolution product where:

$$\psi(y, t; a_2, a_3) = \mathcal{L}^{-1}\{\bar{\psi}(y, q; a_2, a_3)\} = \frac{1}{\pi} \int_0^\infty \int_0^\infty (ur^\alpha \sin \alpha \pi) \psi_1(y, t; a_2, a_3) \exp(-\tau r - ur^\alpha \cos \alpha \pi) dr du, \tag{21}$$

$$\psi_1(y, t; a_2, a_3) = \mathcal{L}^{-1}\left\{\frac{1}{q} \exp\left(-y \sqrt{\frac{a_2 q}{q + a_3}}\right)\right\} = 1 - \frac{2a_2}{\pi} \int_0^\infty \frac{\sin(ys)}{s(a_2 + s^2)} \exp\left(-\frac{a_3 t s^2}{a_2 + s^2}\right) ds, \tag{22}$$

and

$$\chi(t) = \frac{1}{t^\alpha \Gamma(1 - \alpha)}, \tag{23}$$

It is notable here that Equation (20) satisfies all the imposed physical conditions which validate the present solutions.

4.2. Solutions of Momentum Equation

In this section, the same procedure of solutions as in the energy equation is acquired. The Laplace transform technique is applied to Equation (10) and the corresponding initial conditions are used

from Equation (8) which yield to the following non-homogeneous differential equation in the Laplace transform domain

$$\frac{d^2\bar{u}(y, q)}{dy^2} - \left(\frac{b_2q^\alpha + b_3}{q^\alpha + a_3}\right)\bar{u}(y, q) = -\frac{b_1}{q} \exp\left(-y \sqrt{\frac{a_2q^\alpha}{q^\alpha + a_3}}\right); 0 < \alpha \leq 1, \tag{24}$$

where

$$b_1 = \frac{\beta\phi_3 Gr \cos(\delta)}{\phi_1} = \frac{\beta_0\phi_0 a_1}{\phi_1}, b_2 = K_{eff} + b_0, K_{eff} = \frac{\beta\phi_2 M \sin \gamma}{\phi_1} + \frac{\beta}{K}, b_0 = \frac{\beta_0\phi_0 a_1}{\phi_1}, b_3 = K_{eff} a_2.$$

The exact analytical solutions of Equation (24) is given by

$$\begin{aligned} \bar{u}(y, q) = & \frac{q}{q^2 + \omega^2} \exp\left(-y \sqrt{\frac{b_2q^\alpha + b_3}{q^\alpha + a_3}}\right) + \left\{b_1 \left(\frac{q^\alpha + a_3}{b_4q^\alpha - b_3}\right)\right\} \\ & \left\{\frac{1}{q} \exp\left(-y \sqrt{\frac{b_2q^\alpha + b_3}{q^\alpha + a_3}}\right) - \frac{1}{q} \exp\left(-y \sqrt{\frac{a_2q^\alpha}{q^\alpha + a_3}}\right)\right\}; 0 < \alpha \leq 1 \end{aligned} \tag{25}$$

where

$$b_4 = a_2 - b_2.$$

Equation (25) is written in an additional simplified and convenient form as

$$\begin{aligned} \bar{u}(\xi, q) = & \frac{q}{q^2 + \omega^2} \times q\bar{\chi}(q)\bar{\Phi}(y, q, b_2, b_3, a_3) + b_1 \left(\frac{q^\alpha}{b_4q^\alpha - b_3} + \frac{b_1}{b_4q^\alpha - b_3}\right) \\ & \times \left\{\bar{\chi}(q)\bar{\Phi}(y, q, b_2, b_3, a_3) - \bar{\theta}(y, q)\right\}; 0 < \alpha \leq 1 \end{aligned} \tag{26}$$

where

$$\bar{\Phi}(y, q, b_2, b_3, a_3) = \frac{1}{q} \exp\left(-y \sqrt{\frac{b_2q + b_3}{q + a_3}}\right). \tag{27}$$

Upon taking the inverse Laplace to transform, Equation (26) takes the following form

$$\begin{aligned} u(y, t) = & \cos(\omega t) * \Phi(y, t, b_2, b_3, a_3) + \frac{b_1}{b_4} \left\{R_{\alpha, \alpha}\left(\frac{b_3}{b_4}, t\right) + b_1 F_\alpha\left(\frac{b_3}{b_4}, t\right)\right\} \\ & * \left\{\chi(t)\Phi(y, t, b_2, b_3, a_3) - \theta(y, t)\right\}; 0 < \alpha \leq 1 \end{aligned} \tag{28}$$

where $\theta(y, t)$ is presented in Equations (20)–(23) and $R_{\alpha, \nu}(\cdot, \cdot)$ is the Lorenzo and Hartley’s function and $F_\alpha(\cdot, \cdot)$ Robotnov and Hartley’s functions are defined by which are given by [37]

$$R_{\alpha, \nu}(-m, t) = \left(\frac{q^\nu}{q^\alpha + m}\right) = \sum_{n=0}^{\infty} \frac{(-m)^n t^{(n+1)\alpha-1-\nu}}{\Gamma\{(n+1)\alpha - \nu\}}, \tag{29}$$

$$F_\alpha(-m, t) = \left(\frac{1}{q^\alpha + m}\right) = \sum_{n=0}^{\infty} \frac{(-m)^n t^{(n+1)\alpha-1}}{\Gamma\{(n+1)\alpha\}}. \tag{30}$$

and the newly established function $\Phi(y, t, b_2, b_3, a_3)$ is given by:

$$\begin{aligned} \Phi(y, t, b_2, b_3, a_3) = & \mathcal{L}^{-1}\left\{\bar{\Phi}(y, q, b_2, b_3, a_3)\right\} = \\ & \frac{1}{\pi} \int_0^\infty \int_0^\infty (ur^\alpha \sin(\alpha\pi)) \Phi_1(y, t, b_2, b_3, a_3) \exp(-tr - ur^\alpha \cos(\alpha\pi)) dr du, \end{aligned} \tag{31}$$

where:

$$\begin{aligned} \Phi_1(y, t, b_2, b_3, a_3) = & \mathcal{L}^{-1}\left\{\frac{1}{q} \exp\left(-y \sqrt{\frac{b_2q + b_3}{q + a_3}}\right)\right\} = \exp(-y \sqrt{b_2}) \\ & - \int_0^\infty \int_0^\tau \frac{y \sqrt{b_3 - b_2 a_3}}{2(\pi s)^{\frac{1}{2}}} \exp(a_3 s) \times \frac{1}{u} \exp\left(-\frac{y^2}{4u} - b_2 u\right) I_1\left\{2(u(b_3 - b_2 a_3) s)\right\}^{\frac{1}{2}} duds, \end{aligned} \tag{32}$$

and $I_1(\cdot)$ is the Bessel function of the first kind. Equations (20) and (31) complete the solutions of the assumed problem. These solutions are additional reliable, flexible, and generalized which will be discussed in the forthcoming section in detail with a physical explanation.

5. Discussion of Results

In this section, the effects of various flow parameters (for instance, fractional parameter α , the volume concentration of CNTs ϕ , Casson fluid parameter β , magnetic parameter M , angle of inclination of the magnetic field γ , the permeability of porous medium K and thermal Grashof number Gr) are characterized in multiple figures (Figures 3–12) regarding temperature and velocity profiles. For human blood, the Prandtl number is chosen to be 21 and the impacts of all the above-stated parameters are displayed for human blood SWCNTs and human blood MWCNTs.

Figures 3 and 4 display the implications of α on temperature and velocity profiles. These figures show that the temperature and velocity profiles are declining for increasing values of α in both the cases (blood SWCNTs and human blood MWCNTs.). The physical point is the higher values of α relating to the thickness of thermal and momentum boundary layers. Higher values of α reducing the thickness of the thermal boundary layer and therefore the temperature and velocity profiles show a decreasing trend. The trend can be defended by the published work of Ali et al. [40,45]. Besides this, the region of temperature and velocity profiles for $0 < \alpha \leq 1$ is the memory of Atangana–Baleanu fractional derivative, which leads to generality and flexibility of the results. By fixing the values of α , the desired results can be achieved.

The repercussions of ϕ on temperature and velocity profiles are reported in Figures 5 and 6 for SWCNTs and MWCNTs. The conduct of velocity and temperature profiles are reversed. This is due to differences in thermal conductivities and densities as depicted in Tables 1 and 2. The temperature profile involves only thermal conductivities; however, the velocity profile includes both densities and thermal conductivities because the energy equation (Equation (3)) is partially coupled with momentum equations (Equation (2)). $\phi = 0.01, 0.02, 0.03, 0.04$ causes increment to the thermal conductivity of nanofluids (SWCNT and MWCNT nanofluids); consequently, the temperature profile increases. In the case of the velocity profile, the density dominates the thermal conductivities and for $\phi = 0.01, 0.02, 0.03, 0.04$ the nanofluids became denser and more viscous, and accordingly, the velocity profile decelerates, as presented in [16,46]. In addition, Figure 7 is plotted to equate SWCNTs and MWCNTs nanofluids in temperature and velocity profiles. This figure clearly justifies the behavior presented in Figures 5 and 6.

Figure 8 displays the impact of β on the velocity profile. Increasing β reduces the motion of CNT nanofluid because of the reduction in the thickness of momentum boundary layer. Figure 9 discloses the impact of M on the velocity profile for both SWCNTs and MWCNTs. M is a dimensionless number which is accorded with Lorentz force that counters nanofluid velocity. The higher the M higher the Lorentz force, which resists motion. This is why velocity retarded in both the cases of CNTs with increasing M [42]. Likewise, the inclination of a magnetic field γ weakens the impact of M which carries off the Lorentz force. For $\gamma = \pi/2$ (normal magnetic field) the influence of the Lorentz force is the strongest, as depicted in Figure 9 [43].

Figure 11 presents the effect of K on the velocity profile for both cases of CNTs. It is witnessed that greater values of K magnifying the velocity field. This is on account of a reduction of resistance of the porous medium and causes improvement in the thickness of momentum boundary layer. Physically, in this view, the velocity field has enhanced [38]. Finally, Figure 12 depicts the consequences of Gr on the velocity profile. This is the ratio of buoyancy and viscous forces. Higher Gr leads to enhancement in buoyancy forces, which causes the induced flows to grow [35].

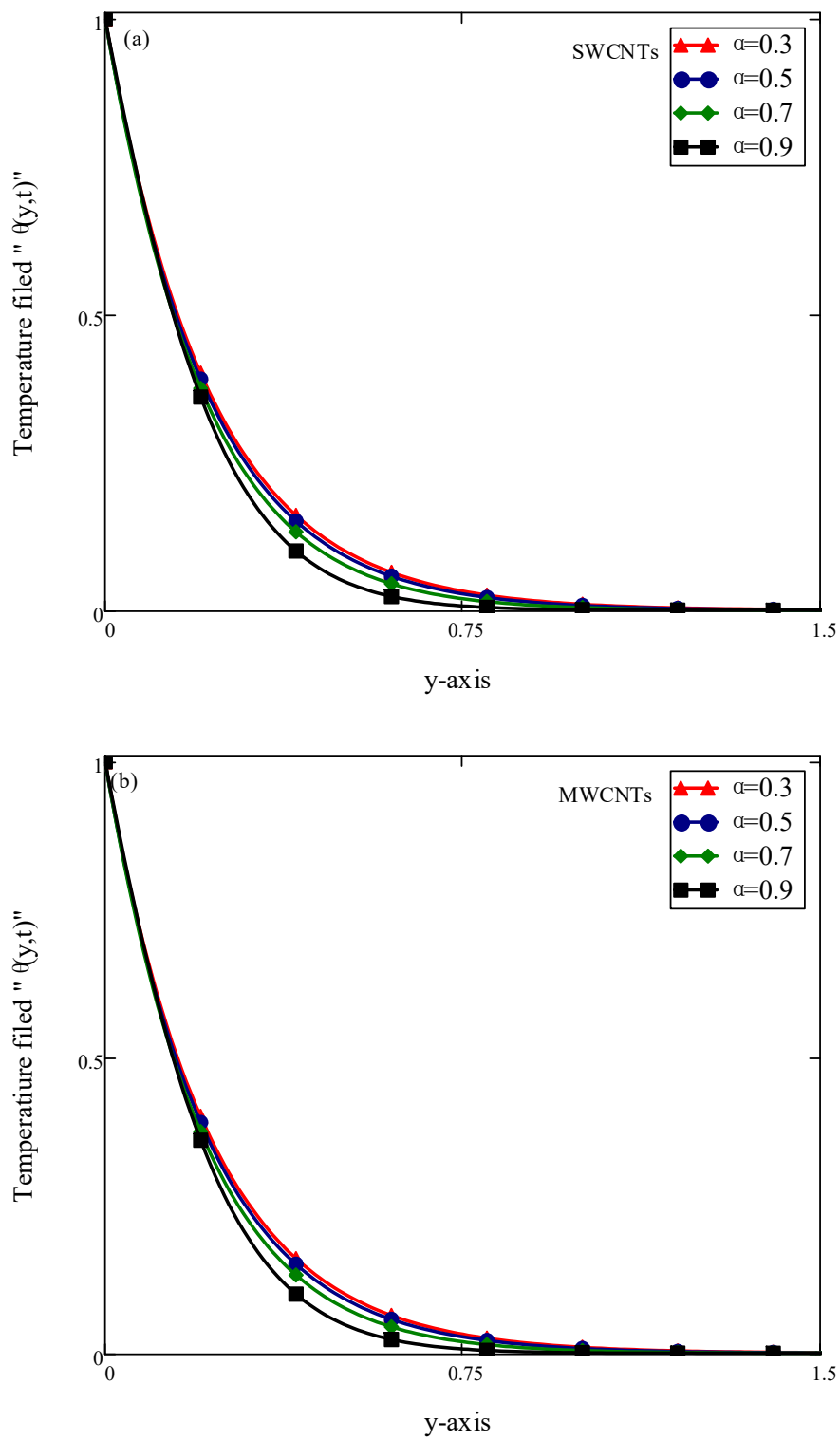


Figure 3. Of α on $\theta(y,t)$ when $t = 0.5$, $Pr = 21$ and $\phi = 0.04$.

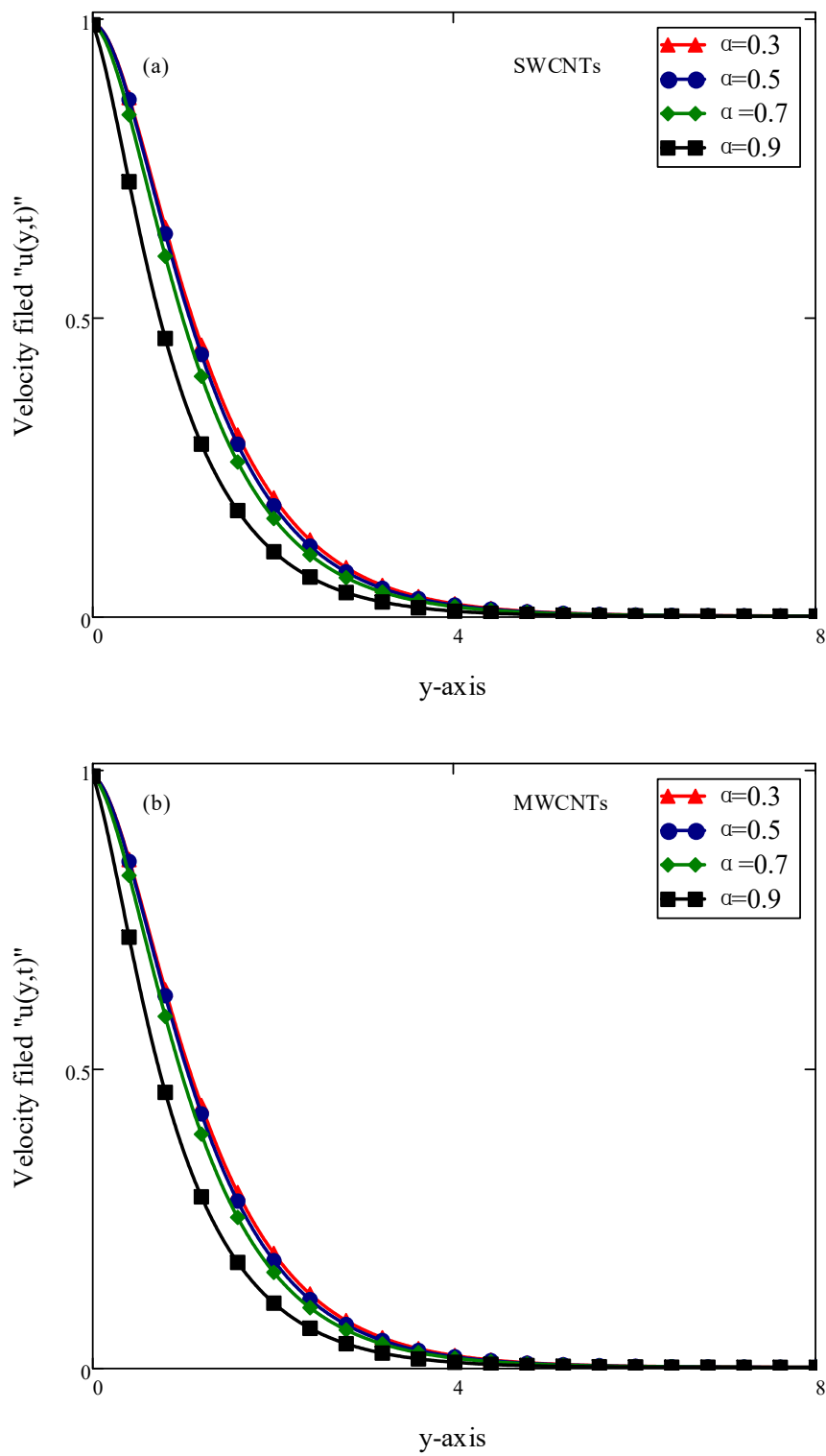


Figure 4. Of α on $u(y, t)$ when $t = 0.5, \beta = 0.5, M = 0.5, \gamma = \pi/2, K = 0.5, Gr = 7.0, Pr = 21$ and $\phi = 0.04$.

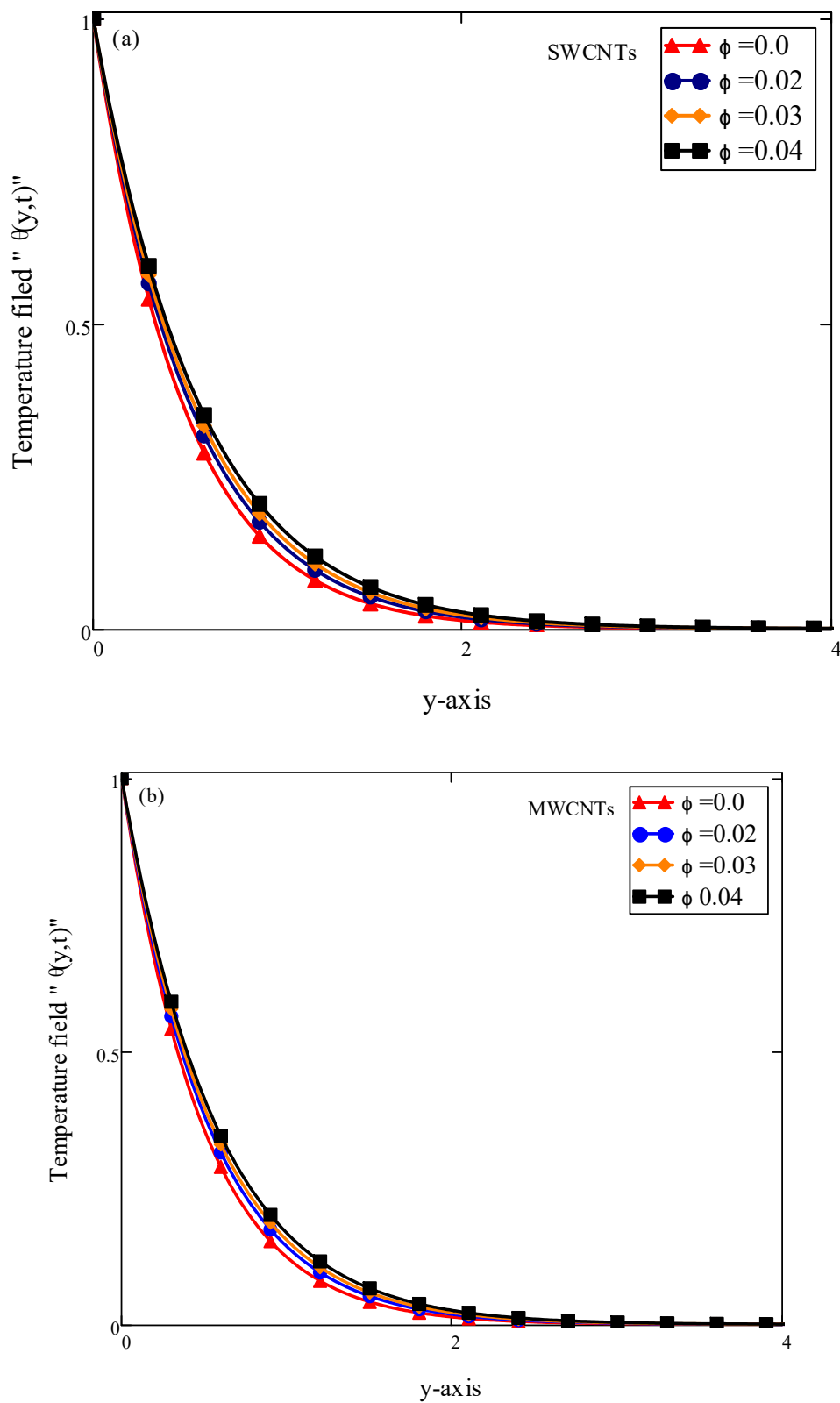


Figure 5. Of ϕ on $\theta(y,t)$ when $t = 0.5$, $Pr = 21$ and $\alpha = 0.5$.

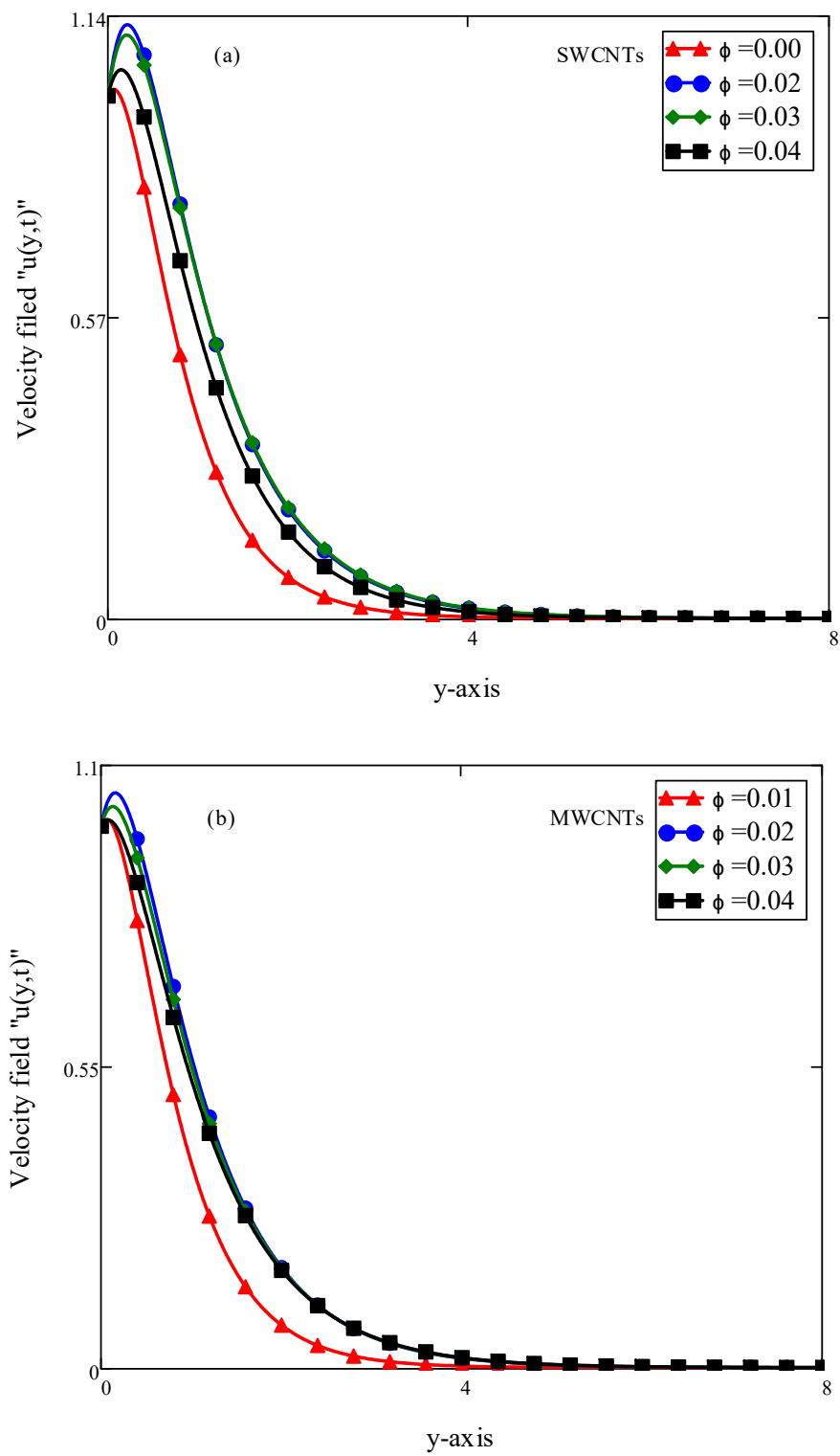


Figure 6. Of ϕ on $u(y,t)$ when $t = 0.5, \beta = 0.5, M = 0.5, \gamma = \pi/2, K = 0.5, Gr = 7.0, Pr = 21$ and $\alpha = 0.5$.

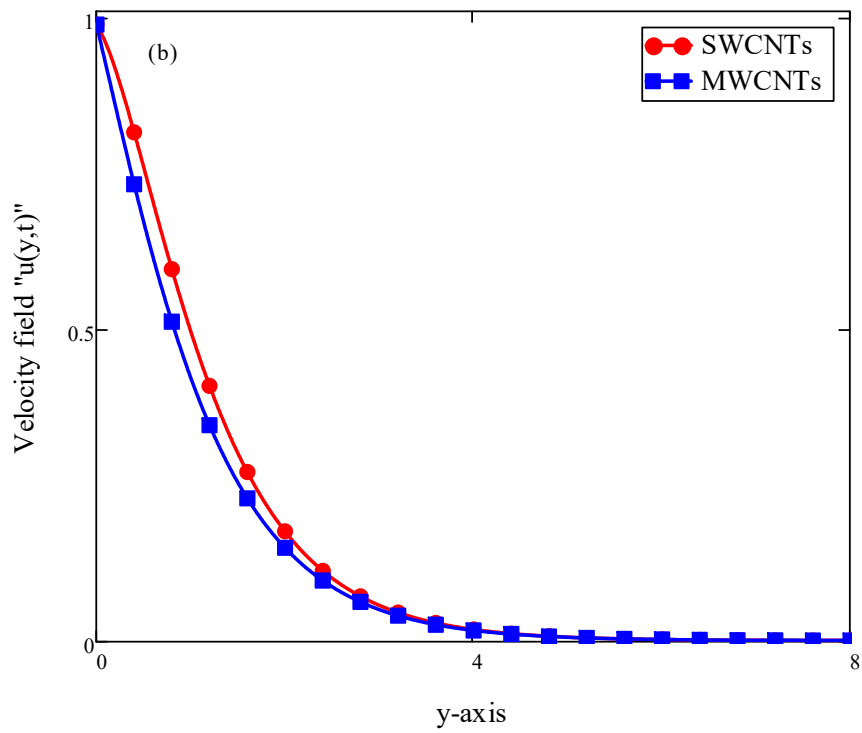
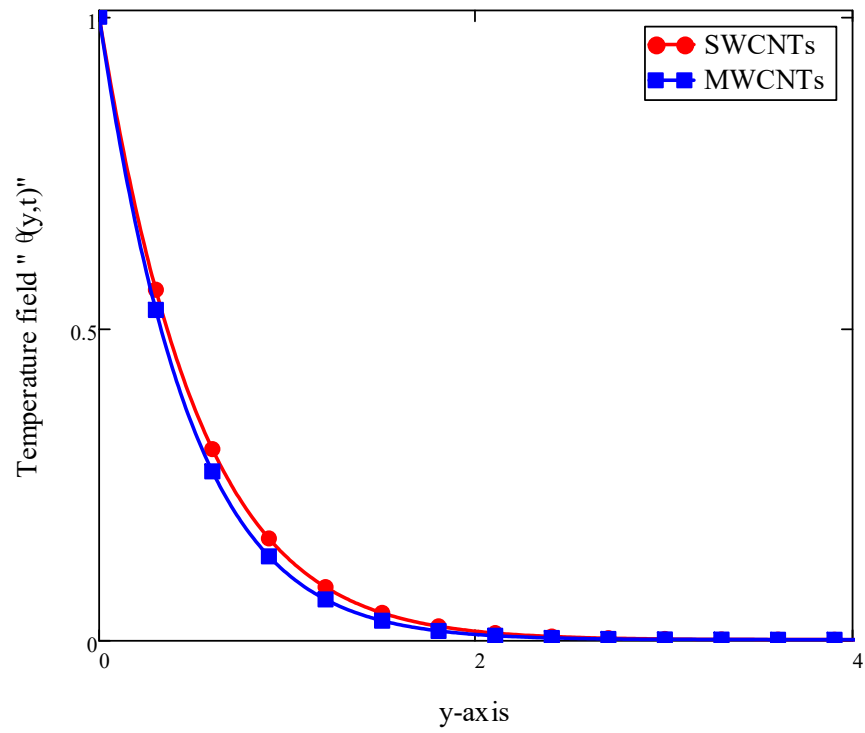


Figure 7. Of $\theta(y,t)$ and $u(y,t)$ for SWCNTs and MWCNTs.

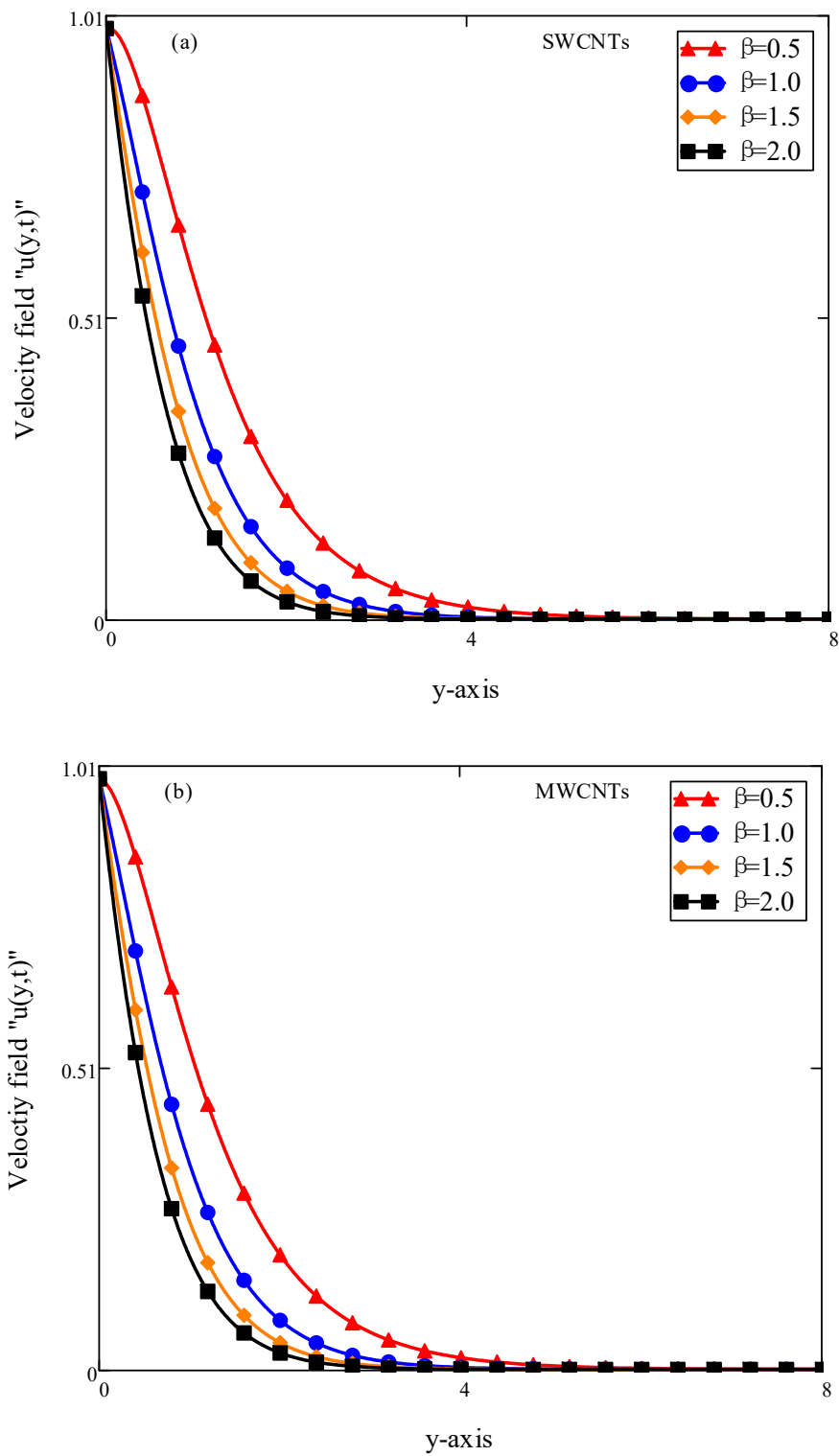


Figure 8. Of β on $u(y,t)$ when $t = 0.5, \phi = 0.04, M = 0.5, \gamma = \pi/2, K = 0.5, Gr = 7.0, Pr = 21$ and $\alpha = 0.5$.

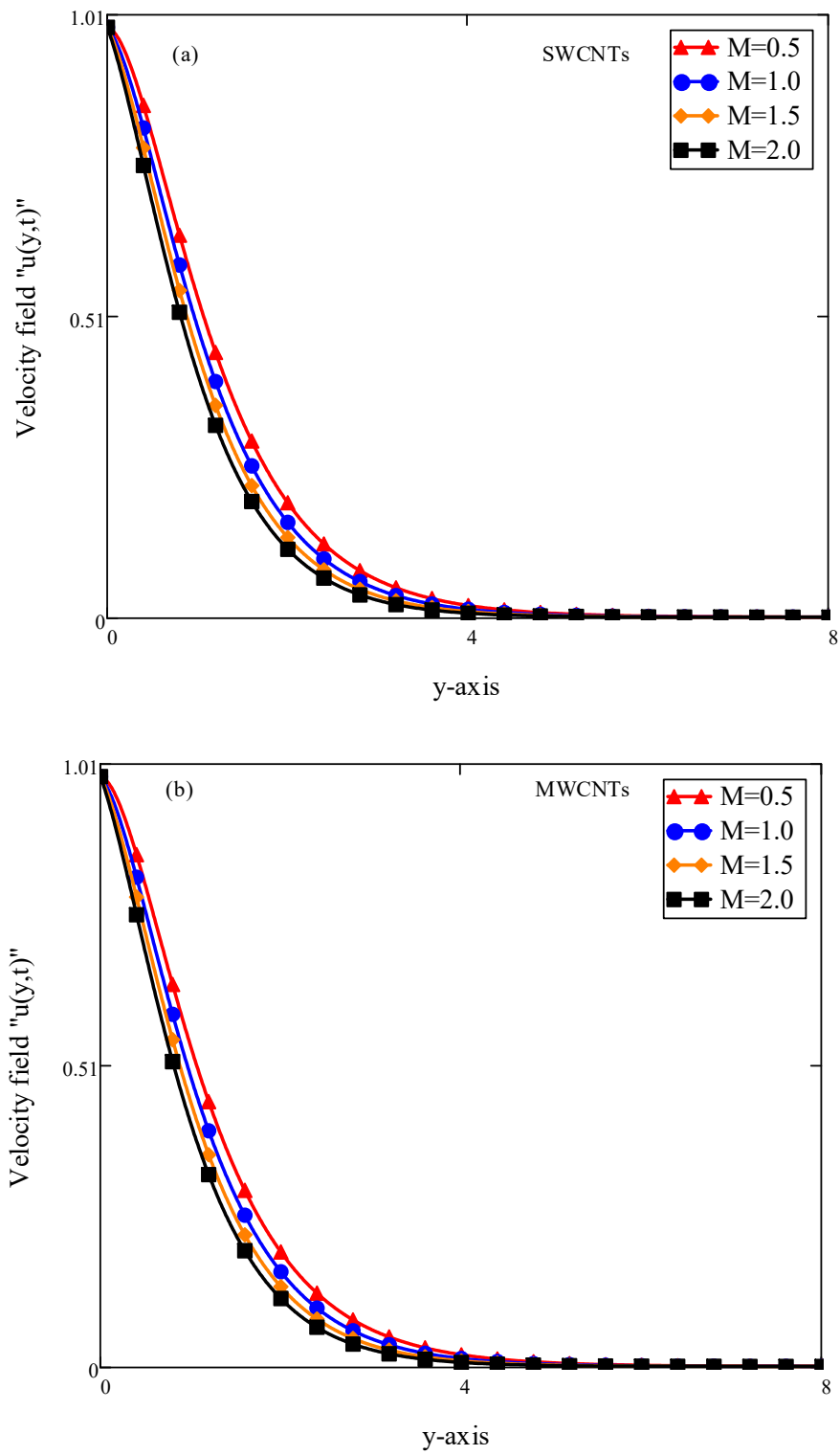


Figure 9. Of M on $u(y,t)$ when $t = 0.5$, $\beta = 0.5$, $\phi = 0.04$, $\gamma = \pi/2$, $K = 0.5$, $Gr = 7.0$, $Pr = 21$ and $\alpha = 0.5$.

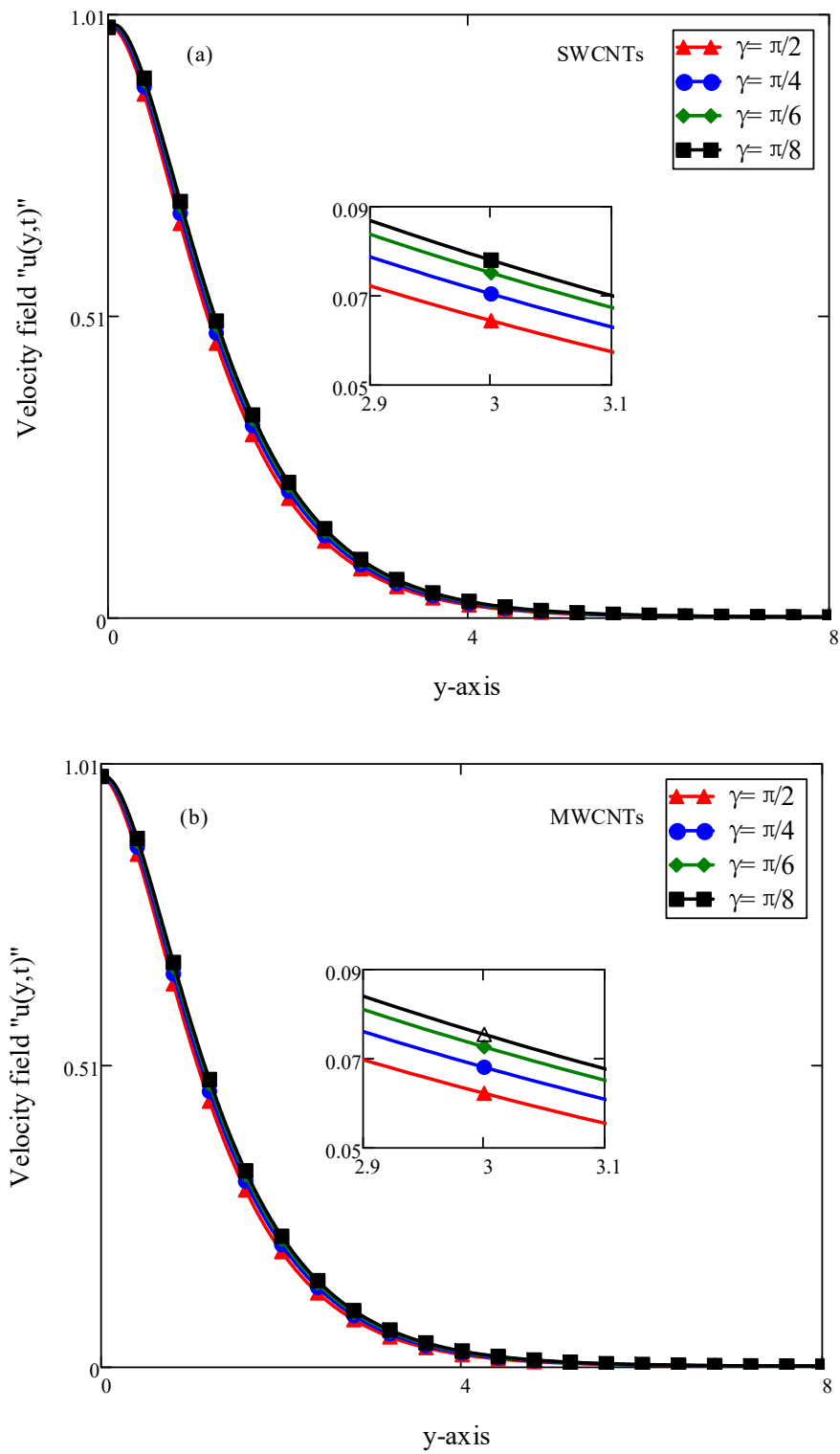


Figure 10. Of γ on $u(y,t)$ when $t = 0.5$, $\phi = 0.04$, $\beta = 0.5$, $M = 0.5$, $K = 0.5$, $Gr = 7.0$, $Pr = 21$ and $\alpha = 0.5$.

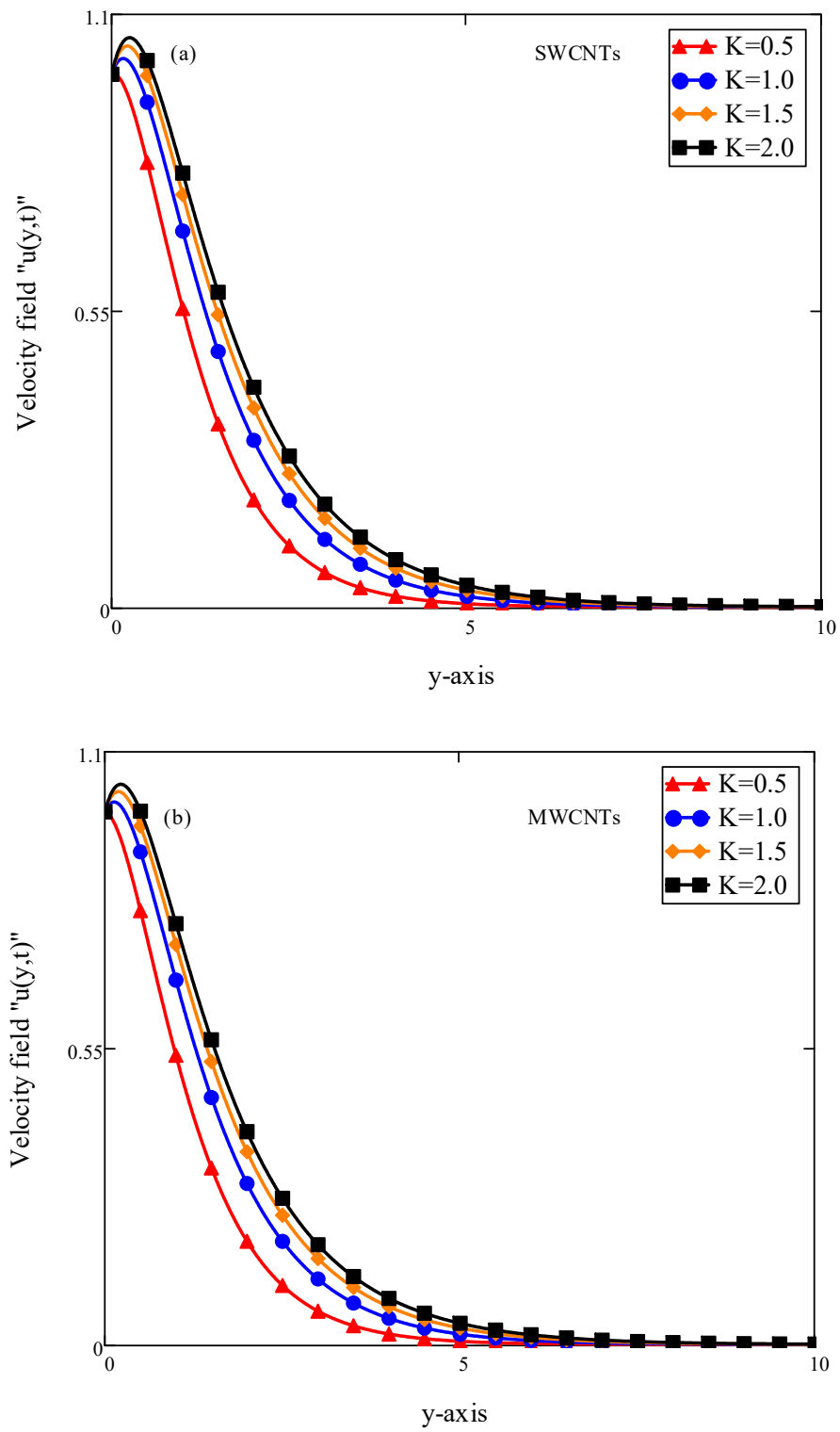


Figure 11. Of K on $u(y,t)$ when $t = 0.5, \phi = 0.04, \beta = 0.5, M = 0.5, \gamma = \pi/2, Gr = 7.0, Pr = 21$ and $\alpha = 0.5$.

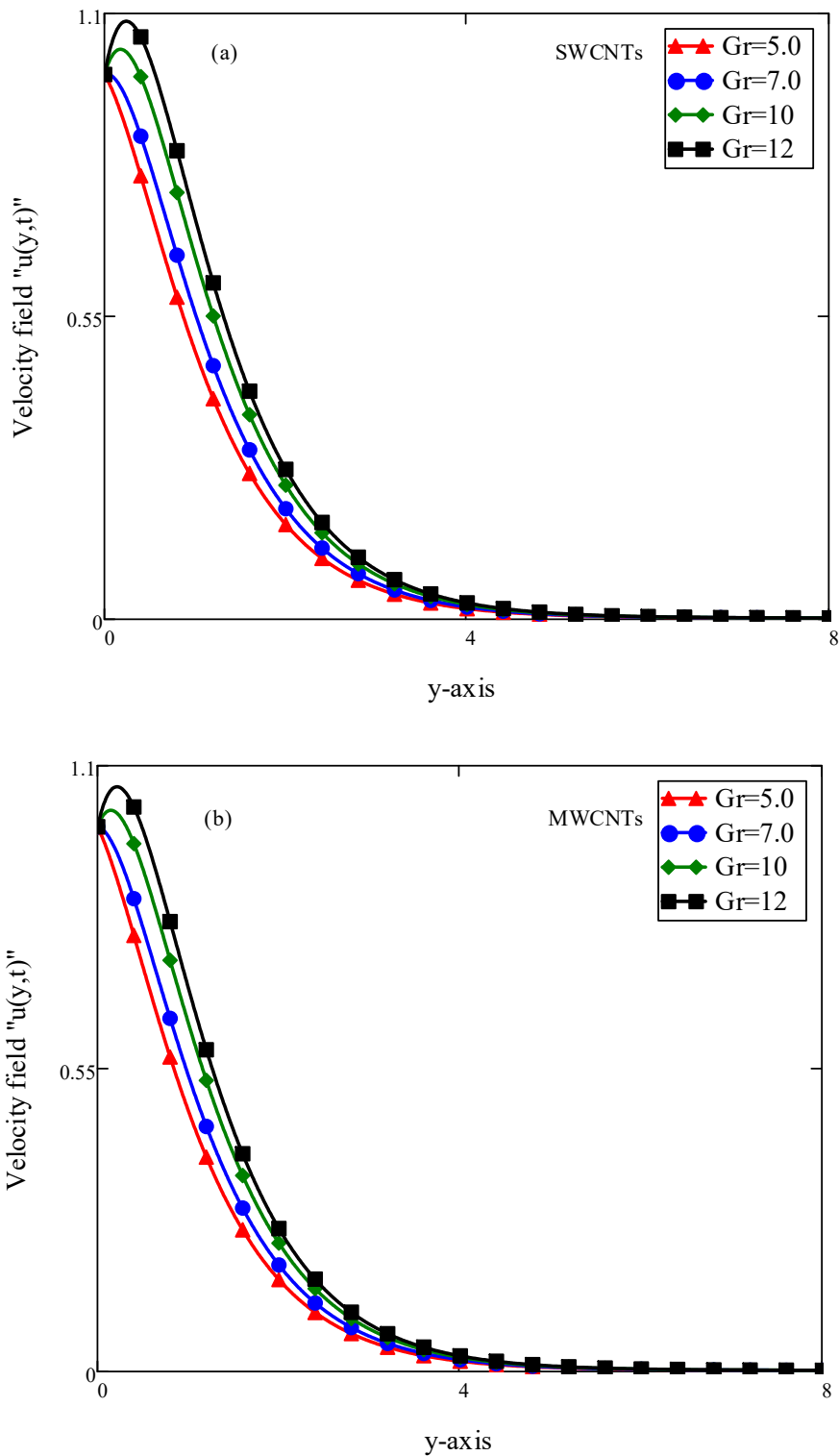


Figure 12. Of Gr on $u(y,t)$ when $t = 0.5$, $\phi = 0.04$, $\beta = 0.5$, $M = 0.5$, $\gamma = \pi/2$, $K = 0.5$, $Pr = 21$ and $\alpha = 0.5$.

6. Concluding Remarks

In the study, a fractional initial and boundary values problem is modeled for the flow of human blood CNT nanofluid over an inclined plate. The effects of an inclined magnetic field and saturated porous medium are considered. The exact analytical solutions for temperature and velocity fields are drafted via the Laplace transform technique. Exact solutions are displayed in various graphs and discussed with physical arguments. The main findings extracted from this study are as follow:

- The fractional solutions for temperature and velocity fields are more general, reliable, and flexible, with memory and heredity properties that can be numerically reduced for any values of $0 < \alpha \leq 1$.
- The temperature profile increase with an increasing volume fraction of CNTs and decreases with increasing fractional parameters (for both cases of CNTs) because of variation in the thermal boundary layer.
- The velocity profile increases with increased permeability of the porous medium and thermal Grashof number, due to the improvement in the velocity boundary layer.
- Nanofluid motion (SWCNTs and MWCTs) retarded with increment in volume concentration of CNTs and magnetic parameters. The normal magnetic field has the strongest resistance to the motion.
- The trends and features of all the physical flow parameters are in excellent agreement with the published work.

Author Contributions: Conceptualization, M.S. and S.S.; methodology, M.S.; software, M.S. and S.S.; validation, M.S., A.R.M.K., N.F.M. and D.L.C.C.; formal analysis, M.S. and S.S.; investigation, M.S. and S.S.; resources, A.R.M.K. and D.L.C.C.; data curation, A.R.M.K. and N.F.M.; writing—original draft preparation, M.S.; writing—review and editing, M.S.; visualization, M.S. and S.S.; supervision, S.S.; project administration, S.S. and D.L.C.C.; funding acquisition, D.L.C.C. All authors have read and agreed to the published version of the manuscript.

Funding: This research was funded by Research Management Centre, Universiti Teknologi Malaysia (UTM) for the financial support through vote numbers 5F278, 5F004, 07G70, 07G72, 07G75, 07G76, 07G77 and 08G33 and “The APC was funded by YUTP 015MC0-011”.

Acknowledgments: The authors would like to acknowledge Ministry of Education (MOHE) and Research Management Centre, Universiti Teknologi Malaysia (UTM) for the financial support through vote numbers 5F278, 5F004, 07G70, 07G72, 07G75, 07G76, 07G77 and 08G33 for this research.

Conflicts of Interest: The authors declare no conflict of interest.

References

1. Shahsavari, A.; Sardari, P.T.; Toghraie, D. Free convection heat transfer and entropy generation analysis of water-Fe₃O₄/CNT hybrid nanofluid in a concentric annulus. *Int. J. Numer. Methods Heat Fluid Flow* **2019**. [[CrossRef](#)]
2. Talebizadehsardari, P.; Shahsavari, A.; Toghraie, D.; Barnoon, P. An experimental investigation for study the rheological behavior of water-carbon nanotube/magnetite nanofluid subjected to a magnetic field. *Phys. A Stat. Mech. Appl.* **2019**, *534*, 122129. [[CrossRef](#)]
3. Mahanthesh, B.; Lorenzini, G.; Oudina, F.M.; Animasaun, I.L. Significance of exponential space-and thermal-dependent heat source effects on nanofluid flow due to radially elongated disk with Coriolis and Lorentz forces. *J. Therm. Anal. Calorim.* **2019**, 1–8. [[CrossRef](#)]
4. Liou, T.-M.; Wei, T.-C.; Wang, C.-S. Investigation of nanofluids on heat transfer enhancement in a louvered microchannel with lattice Boltzmann method. *J. Therm. Anal. Calorim.* **2019**, *135*, 751–762. [[CrossRef](#)]
5. Mebarek-Oudina, F.; Bessaïh, R. Numerical simulation of natural convection heat transfer of copper-water nanofluid in a vertical cylindrical annulus with heat sources. *Thermophys. Aeromechanics* **2019**, *26*, 325–334. [[CrossRef](#)]
6. Raza, J.; Mebarek-Oudina, F.; Mahanthesh, B. Magnetohydrodynamic flow of nano Williamson fluid generated by stretching plate with multiple slips. *Multidiscip. Modeling Mater. Struct.* **2019**, *15*, 871–894. [[CrossRef](#)]
7. Álvarez-Regueiro, E.; Vallejo, J.P.; Fernández-Seara, J.; Fernández, J.; Lugo, L. Experimental convection heat transfer analysis of a nano-enhanced industrial coolant. *Nanomaterials* **2019**, *9*, 267. [[CrossRef](#)]
8. O Alzahrani, E.; Shah, Z.; Alghamdi, W.; Zaka Ullah, M. Darcy–Forchheimer Radiative Flow of Micropolar CNT Nanofluid in Rotating Frame with Convective Heat Generation/Consumption. *Processes* **2019**, *7*, 666. [[CrossRef](#)]
9. Gul, T.; Khan, M.A.; Noman, W.; Khan, I.; Abdullah Alkanhal, T.; Tlili, I. Fractional order forced convection carbon nanotube nanofluid flow passing over a thin needle. *Symmetry* **2019**, *11*, 312. [[CrossRef](#)]

10. Hussanan, A.; Khan, I.; Gorji, M.R.; Khan, W.A. CNT S-Water-Based Nanofluid Over a Stretching Sheet. *BioNanoScience* **2019**, *9*, 21–29. [[CrossRef](#)]
11. Jabbari, F.; Rajabpour, A.; Saedodin, S. Viscosity of carbon nanotube/water nanofluid. *J. Therm. Anal. Calorim.* **2019**, *135*, 1787–1796. [[CrossRef](#)]
12. Kumam, P.; Shah, Z.; Dawar, A.; Rasheed, H.U.; Islam, S. Entropy generation in MHD radiative flow of CNTs Casson nanofluid in rotating channels with heat source/sink. *Math. Probl. Eng.* **2019**, *2019*. [[CrossRef](#)]
13. Murshed, S.S.; De Castro, C.N. Superior thermal features of carbon nanotubes-based nanofluids—A review. *Renew. Sustain. Energy Rev.* **2014**, *37*, 155–167. [[CrossRef](#)]
14. Motevasel, M.; Soleimanyazar, A.; Jamialahmadi, M. Forced Convective Heat Transfer of Nano fluids: A Review of the Recent Literature. *Am. J. Oil Chem. Technol.* **2014**, *2*, 105–118.
15. Sundar, L.S.; Sharma, K.; Naik, M.; Singh, M.K. Empirical and theoretical correlations on viscosity of nanofluids: A review. *Renew. Sustain. Energy Rev.* **2013**, *25*, 670–686. [[CrossRef](#)]
16. Saqib, M.; Khan, I.; Shafie, S. Application of Atangana–Baleanu fractional derivative to MHD channel flow of CMC-based-CNT's nanofluid through a porous medium. *Chaos Solitons Fractals* **2018**, *116*, 79–85. [[CrossRef](#)]
17. Murshed, S.S.; De Castro, C.N.; Lourenço, M.; Lopes, M.; Santos, F. A review of boiling and convective heat transfer with nanofluids. *Renew. Sustain. Energy Rev.* **2011**, *15*, 2342–2354. [[CrossRef](#)]
18. Xie, H.; Chen, L. Review on the preparation and thermal performances of carbon nanotube contained nanofluids. *J. Chem. Eng. Data* **2011**, *56*, 1030–1041. [[CrossRef](#)]
19. Sarafraz, M.; Nikkhab, V.; Nakhjavani, M.; Arya, A. Fouling formation and thermal performance of aqueous carbon nanotube nanofluid in a heat sink with rectangular parallel microchannel. *Appl. Therm. Eng.* **2017**, *123*, 29–39. [[CrossRef](#)]
20. Selimefendigil, F.; Öztop, H.F. Corrugated conductive partition effects on MHD free convection of CNT-water nanofluid in a cavity. *Int. J. Heat Mass Transf.* **2019**, *129*, 265–277. [[CrossRef](#)]
21. Mohd-Ghazali, N.; Estellé, P.; Halelfadl, S.; Maré, T.; Siong, T.C.; Abidin, U. Thermal and hydrodynamic performance of a microchannel heat sink with carbon nanotube nanofluids. *J. Therm. Anal. Calorim.* **2019**, *138*, 937–945. [[CrossRef](#)]
22. Abdeen, D.H.; Atieh, M.A.; Merzougui, B.; Khalfaoui, W. Corrosion Evaluation of 316L Stainless Steel in CNT-Water Nanofluid: Effect of CNTs Loading. *Materials* **2019**, *12*, 1634. [[CrossRef](#)] [[PubMed](#)]
23. Abro, K.A.; Atangana, A. A comparative study of convective fluid motion in rotating cavity via Atangana–Baleanu and Caputo–Fabrizio fractal–fractional differentiations. *Eur. Phys. J. Plus* **2020**, *135*, 226. [[CrossRef](#)]
24. Atangana, A.; Aguilar, J.F.G.; Kolade, M.O.; Hristov, J.Y. Fractional differential and integral operators with non-singular and non-local kernel with application to nonlinear dynamical systems. *CSF* **2020**, *132*, 109493. [[CrossRef](#)]
25. Dubey, V.P.; Kumar, R.; Kumar, D.; Khan, I.; Singh, J. An efficient computational scheme for nonlinear time fractional systems of partial differential equations arising in physical sciences. *Adv. Differ. Equ.* **2020**, *2020*, 46. [[CrossRef](#)]
26. Heydari, M.; Atangana, A. An optimization method based on the generalized Lucas polynomials for variable-order space-time fractional mobile-immobile advection-dispersion equation involving derivatives with non-singular kernels. *Chaos Solitons Fractals* **2020**, *132*, 109588. [[CrossRef](#)]
27. Suthar, D.; Khan, A.; Alaria, A.; Purohit, S.; Singh, J. Extended Bessel-Maitland function and its properties pertaining to integral transforms and fractional calculus. *AIMS Math.* **2020**, *5*, 1400. [[CrossRef](#)]
28. Veerasha, P.; Prakasha, D.; Singh, J. Solution for fractional forced KdV equation using fractional natural decomposition method. *AIMS Math.* **2019**, *5*, 798–810. [[CrossRef](#)]
29. Veerasha, P.; Prakasha, D.; Singh, J. A novel approach for nonlinear equations occurs in ion acoustic waves in plasma with Mittag-Leffler law. *Eng. Comput.* **2020**. [[CrossRef](#)]
30. Podlubny, I. *Fractional Differential Equations: An Introduction to Fractional Derivatives, Fractional Differential Equations, to Methods of Their Solution and Some of Their Applications*; Elsevier: Amsterdam, The Netherlands, 1998.
31. Caputo, M. Linear models of dissipation whose Q is almost frequency independent. *Ann. Geophys.* **1966**, *19*, 383–393. [[CrossRef](#)]
32. Caputo, M. Linear models of dissipation whose Q is almost frequency independent—II. *Geophys. J. Int.* **1967**, *13*, 529–539. [[CrossRef](#)]

33. Caputo, M.; Fabrizio, M. A new definition of fractional derivative without singular kernel. *Progr. Fract. Differ. Appl.* **2015**, *1*, 1–13.
34. Atangana, A.; Doungmo Goufo, E. A model of the groundwater flowing within a leaky aquifer using the concept of local variable order derivative. *J. Nonlinear Sci. Appl.* **2015**, *8*, 763–775. [[CrossRef](#)]
35. Ali, F.; Sheikh, N.A.; Khan, I.; Saqib, M. Solutions with Wright function for time fractional free convection flow of Casson fluid. *Arab. J. Sci. Eng.* **2017**, *42*, 2565–2572. [[CrossRef](#)]
36. Khalid, A.; Khan, I.; Khan, A.; Shafie, S.; Tlili, I. Case study of MHD blood flow in a porous medium with CNTs and thermal analysis. *Case Stud. Therm. Eng.* **2018**, *12*, 374–380. [[CrossRef](#)]
37. Saqib, M.; Khan, I.; Shafie, S. Generalized magnetic blood flow in a cylindrical tube with magnetite dusty particles. *J. Magn. Magn. Mater.* **2019**, *484*, 490–496. [[CrossRef](#)]
38. Ali, F.; Saqib, M.; Khan, I.; Sheikh, N.A.; Jan, S.A.A. Exact analysis of MHD flow of a Walters'-B fluid over an isothermal oscillating plate embedded in a porous medium. *Eur. Phys. J. Plus* **2017**, *132*, 95. [[CrossRef](#)]
39. Sheikh, N.A.; Ching, D.L.C.; Khan, I.; Kumar, D.; Nisar, K.S. A new model of fractional Casson fluid based on generalized Fick's and Fourier's laws together with heat and mass transfer. *Alex. Eng. J.* **2019**. [[CrossRef](#)]
40. Ali, F.; Saqib, M.; Khan, I.; Sheikh, N.A. Application of Caputo-Fabrizio derivatives to MHD free convection flow of generalized Walters'-B fluid model. *Eur. Phys. J. Plus* **2016**, *131*, 377. [[CrossRef](#)]
41. Saqib, M.; Khan, I.; Shafie, S.; Qushairi, A. Recent Advancement in Thermophysical Properties of Nanofluids and Hybrid nanofluids: An Overviews. *City Univ. Int. J. Comput. Anal.* **2020**, *1*, 16–25.
42. Jan, S.A.A.; Ali, F.; Sheikh, N.A.; Khan, I.; Saqib, M.; Gohar, M. Engine oil based generalized brinkman-type nano-liquid with molybdenum disulphide nanoparticles of spherical shape: Atangana-Baleanu fractional model. *Numer. Methods Partial Differ. Equ.* **2018**, *34*, 1472–1488. [[CrossRef](#)]
43. Shafie, S.; Saqib, M.; Khan, I.; Qushairi, A. Mixed Convection Flow of Brinkman Type Hybrid Nanofluid Based on Atangana-Baleanu Fractional Model. In Proceedings of the Journal of Physics: Conference Series, Kuantan, Malaysia, 23–25 July 2019; p. 012041.
44. Saqib, M.; Khan, I.; Shafie, S. Shape Effect in Magnetohydrodynamic Free Convection Flow of Sodium Alginate-Ferrimagnetic Nanofluid. *J. Therm. Sci. Eng. Appl.* **2019**, *11*. [[CrossRef](#)]
45. Ali, F.; Sheikh, N.A.; Khan, I.; Saqib, M. Magnetic field effect on blood flow of Casson fluid in axisymmetric cylindrical tube: A fractional model. *J. Magn. Magn. Mater.* **2017**, *423*, 327–336. [[CrossRef](#)]
46. Khan, I.; Saqib, M.; Alqahtani, A.M. Channel flow of fractionalized H₂O-based CNTs nanofluids with Newtonian heating. *Discret. Contin. Dyn. Syst. S* **2019**, *13*, 769–779. [[CrossRef](#)]



© 2020 by the authors. Licensee MDPI, Basel, Switzerland. This article is an open access article distributed under the terms and conditions of the Creative Commons Attribution (CC BY) license (<http://creativecommons.org/licenses/by/4.0/>).